ARTICLE IN PRESS

Nuclear Inst. and Methods in Physics Research, A ▮ (▮▮▮▮) ▮▮▮–▮▮▮

Contents lists available at ScienceDirect

Nuclear Inst. and Methods in Physics Research, A

journal homepage: www.elsevier.com/locate/nima

Spatially resolved measurement of wideband prompt gamma-ray emission toward on-line monitor for the future proton therapy

A. Koide [a,*], J. Kataoka [a], T. Taya [a], Y. Iwamoto [a], K. Sueoka [a], S. Mochizuki [a], M. Arimoto [a], T. Inaniwa [b]

[a] Research Institute for Science and Engineering, Waseda University, 3-4-1 Ohkubo, Shinjuku, Tokyo, Japan
[b] National Institute of Radiological Sciences, 4-9-1 Anagawa, Inage-ku, Chiba-shi, Chiba, Japan

ARTICLE INFO

Keywords:
Particle therapy
Prompt gamma rays
Compton camera

ABSTRACT

In proton therapy, the delivered dose should be monitored to a high degree of accuracy to avoid unnecessary exposure to healthy tissues and critical organs. Although positron emission tomography (PET) is most frequently used to verify the proton range, the nuclear reactions between protons and nuclei that generate positrons do not necessarily correspond to the actual proton range. Moreover, such imaging must be conducted after the treatment irradiation, because a PET gantry cannot be used in conjunction with a proton therapy beam. In this paper, we studied one-dimensional (1D) and two-dimensional (2D) distributions of prompt gamma rays of various energies, to determine the most suitable energy window for online monitoring in proton therapy. After an initial simulation study using the particle and heavy ion transport code system (PHITS), we irradiated a poly(methyl methacrylate) (PMMA) phantom with a 70-MeV proton beam to mimic proton range verification in a clinical situation. Using a newly developed Compton camera, we have experimentally confirmed for the first time that 4.4-MeV gamma rays emitted from ^{12}C and ^{16}O match the exact position of the Bragg peak in proton range verification.

© 2017 Published by Elsevier B.V.

1. Introduction

Radiation therapy utilizes ionizing radiation to damage malignant cells. Therapy that specifically uses charged particles, such as protons or heavy ions, is called particle therapy. Particle therapy can target the dose to the tumor while minimizing damage to healthy tissues, owing to the dose being concentrated at the Bragg peak, which corresponds to the range of the particle beam. Immense damage may be caused to healthy tissues if the irradiation is inaccurately performed. Therefore, high precision is required in both treatment planning and dose delivery. Positron emission tomography (PET) is widely used to verify the proton range, but its use is limited to offline imaging because a PET gantry cannot be used in conjunction with the clinical beam. Some research groups have developed an online system that uses a planar PET scanner [1,2], but a fundamental problem is that the nuclear reactions that produce β^+-emitting nuclei differ from the energy loss of incident protons; in fact, the position of the annihilation gamma-ray distribution peak substantially differs from that of the Bragg peak [3,4].

Very recently, alternative methods that utilizes prompt gamma rays have been proposed to verify the proton range in real time during therapy, e.g., using a Compton camera [5–7], slit camera [8], or gamma camera with time of flight (TOF) capability [9]. However, the question of which prompt gamma-ray energy is most suitable for proton range verification remains unanswered. Numerous attempts are in progress but remain limited to simulation studies, as it is difficult to directly image high-energy gamma rays, especially those above 1 MeV due to multiple interactions or escape event in a detector.

In this paper, we systematically investigated the energy spectrum and spatial distribution of prompt gamma rays, for use as a new tool for online monitoring during proton therapy. First, we measured the overall spectrum of prompt gamma rays emitted from a Poly(methyl methacrylate) (PMMA) phantom irradiated by 70-MeV protons, using a high purity germanium (HPGe) detector. Next, we simulated a one-dimensional (1D) profile of various nuclear emission lines in the range of 10 keV–5 MeV along the proton path, and compared them with experimental results obtained using a Pb slit collimator. Finally, we present the first preliminary imaging test of prompt gamma rays, using a newly developed Compton camera. Both the 1D profile and two-dimensional (2D) images indicate that 4.4-MeV gamma rays, emitted

* Corresponding author.
E-mail address: ayako-k@asagi.waseda.jp (A. Koide).

https://doi.org/10.1016/j.nima.2017.10.020
Received 19 September 2017; Received in revised form 9 October 2017; Accepted 9 October 2017
Available online xxxx
0168-9002/© 2017 Published by Elsevier B.V.

Please cite this article in press as: A. Koide, et al., Spatially resolved measurement of wideband prompt gamma-ray emission toward on-line monitor for the future proton therapy, Nuclear Inst. and Methods in Physics Research, A (2017), https://doi.org/10.1016/j.nima.2017.10.020.

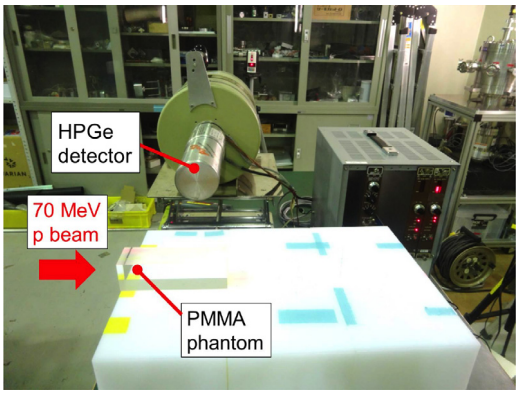

Fig. 1. Experimental set-up for measuring the energy spectrum of prompt gamma rays with an HPGe detector. The distance between the detector and phantom was set to 25 cm to avoid saturation of the data acquisition system, which would occur due to the very high count rate. We obtained the spectrum for 10 min during irradiation, and accumulated the off-beam spectrum for an additional 10 min, after the beam had been switched off.

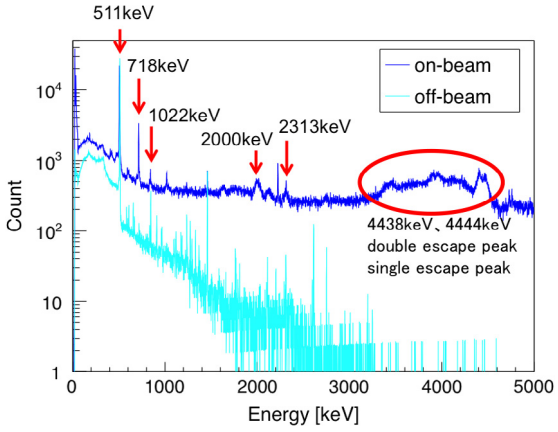

Fig. 2. Energy spectra of the gamma rays emitted during proton irradiation of the PMMA phantom. The blue and cyan histograms represent the on-beam and off-beam spectra, respectively. (For interpretation of the references to color in this figure legend, the reader is referred to the web version of this article.)

from ^{12}C and ^{16}O, are a potential tool for range verification in proton therapy.

2. The energy spectrum of prompt gamma rays

2.1. Experimental setup

First, we obtained the energy spectrum of prompt gamma rays emitted during the proton beam irradiation. We irradiated a PMMA phantom with a 70-MeV proton beam at the Ring Cyclotron facility at the National Institute of Radiological Sciences, Japan. The spectrum of prompt gamma rays was obtained in the range of 10–5000 keV, using a HPGe detector (EG&G GEM-40190-P-S). The detector had a cylindrical HPGe crystal of diameter 5.9 cm and height 8.08 cm. The PMMA phantom had dimensions of 3 cm × 3 cm × 10 cm. The intensity and exposure time of the proton beam were 3 pA and 10 min, respectively. The experimental setup is shown in Fig. 1. The HPGe detector was set perpendicular to the beam axis. The center of the detector's field of view was exactly aligned with the position of the Bragg peak of the incident proton beam. The distance between the detector and the phantom was 25 cm.

2.2. Result

Fig. 2 compares the energy spectra recorded for the on-beam and off-beam conditions. These spectra were corrected to account for the HPGe detector efficiency as calculated by a Geant4 simulation. Various gamma-emission lines are present, in addition to continuum emissions, only in the on-beam spectrum. The 511-keV annihilation gamma rays and other weak lines, mostly due to contamination from the room background, can be seen in both spectra.

We verified lines at 718, 1022, 2000, 2313, 4438, and 4444 keV corresponding to prompt gamma rays. The 4438-keV and 4444-keV gamma rays cannot be distinguished because of Doppler broadening [10], and are therefore, collectively referred to as 4.4-MeV prompt gamma rays. The peaks at 3.4 and 3.9 MeV are the double escape and single escape peaks of 4.4-MeV gamma rays, respectively.

3. 1D distributions along the proton path

3.1. Simulation

Next, we simulated 1D distributions of the various prompt gamma-ray line emissions seen in Fig. 2 along the proton path, using the particle and heavy ion transport code system (PHITS) [11]. The PMMA phantom matched that in the experiment. We selected the 718-keV, 1022-keV, and 4.4-MeV lines as potential windows, these being the most prominent gamma-ray peaks. The 2000-keV and 2313-keV peaks are difficult to distinguish from the 2225-keV line due to neutron capture and were, therefore, not considered. In addition, we evaluated a 1D profile of 511-keV annihilation gamma rays, most commonly used for proton range verification, as a reference. The result is shown in Fig. 3, which compares the distribution of gamma rays with the dose distribution of the proton beam.

The 511-keV profile peaks 15 mm from the entry face of the PMMA phantom, beyond which the distribution sharply falls off towards the Bragg peak, which is located at 35 mm. Similarly, the overall shapes of the 1D profiles of the 718-keV and 1022-keV peaks did not coincide with that of the proton dose distribution. In contrast, the peak of the 4.4-MeV prompt gamma-ray emission coincided with the Bragg peak of the incident proton, as has been noted in the literature [7].

3.2. Experiments

A corresponding experiment was performed using a detector with a narrow Pb slit collimator. The phantom was scanned along the proton path and the gamma-ray spectrum was obtained at each scanned position. Near the Bragg peak, located at 35 mm, we moved the detector in 2-mm steps to obtain accurate data. At other positions, we used a 4-mm step. The detector was collimated with a 30-cm lead block and 2.5-cm copper block to reduce the background. The copper blocks were placed to reduce the K_α emissions from the lead. The width of the slit collimator was 4 mm. For the 4.4-MeV prompt gamma distribution, we set the energy window as 3000–5000 keV, in order to include both the double and single escape peaks. Fig. 4 shows the 1D profile, i.e., the variation of counts, for this energy range at positions between 8 ± 2 mm and 40 ± 2 mm. From these values we have subtracted the counts recorded at 44 ± 2 mm, which serve as a background. For example, the total photon count measured near the Bragg peak (32 ± 2 mm) was 21 726, of which 9200 ± 100 were estimated as background contamination. The peak is at 32 ± 2 mm, consistent with the theoretical position of the Bragg peak.

4. Imaging of prompt gamma rays

We have shown that the 1D distribution for 4.4-MeV prompt gamma rays, including the position of its peak, closely follows the proton dose distribution. In an actual clinical setting, however, the exposure of the proton beam must be spatially distributed according to the shape of

Please cite this article in press as: A. Koide, et al., Spatially resolved measurement of wideband prompt gamma-ray emission toward on-line monitor for the future proton therapy, Nuclear Inst. and Methods in Physics Research, A (2017), https://doi.org/10.1016/j.nima.2017.10.020.

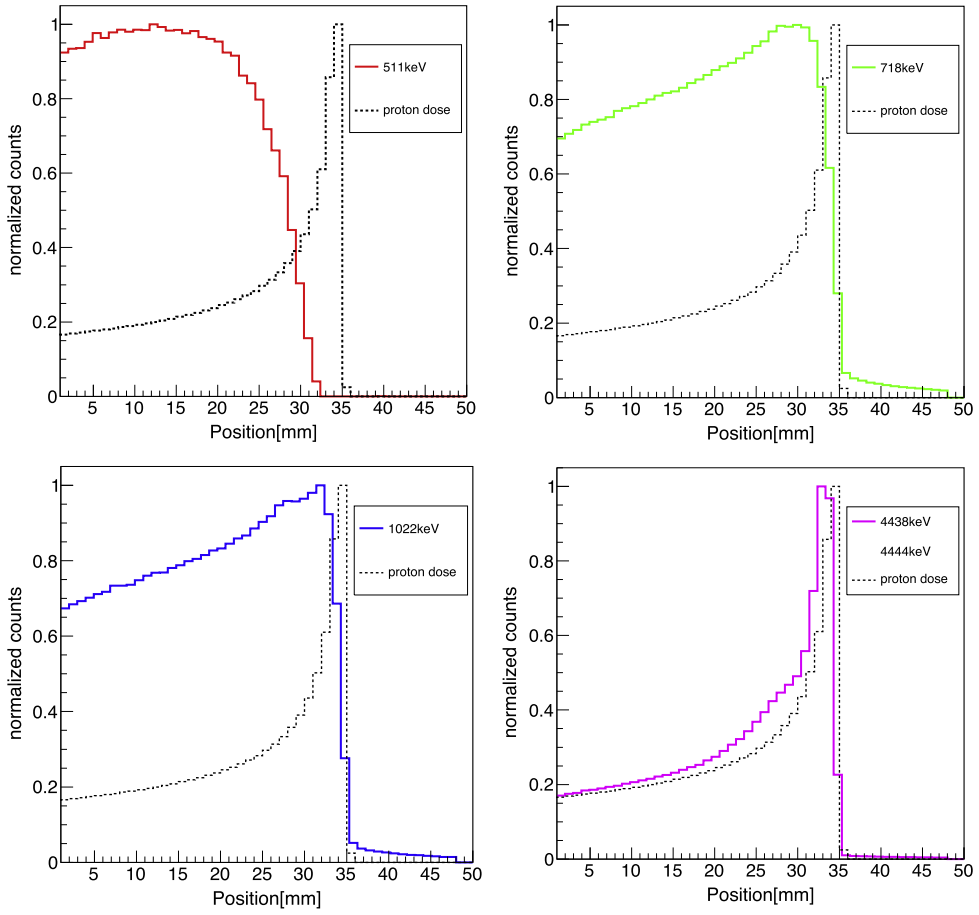

Fig. 3. Simulated 1D distribution of prompt gamma rays along the proton path, obtained using the PHITS code. *Top left*: 511-keV annihilation gamma rays, *Top right*: 718-keV prompt gamma rays, *Bottom left*: 1022-keV prompt gamma rays, *Bottom right*: 4444-keV prompt gamma rays.

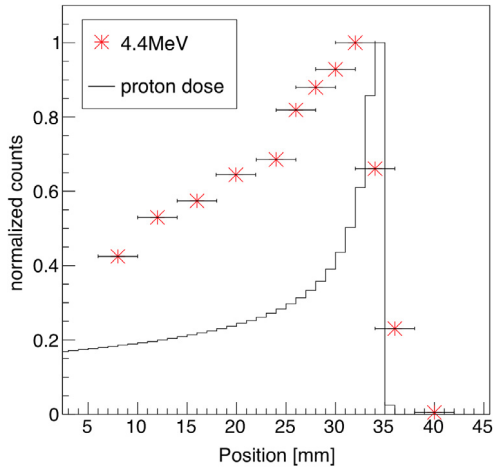

Fig. 4. The 1D distribution of 4.4-MeV prompt gamma rays as measured with a Pb slit collimator. For reference, the distribution is shown as a solid black line which is calculated using the Geant4 simulation. The counts recorded at positions between 8 ± 2 mm and 40 ± 2 mm are indicated by red markers. (For interpretation of the references to color in this figure legend, the reader is referred to the web version of this article.)

the tumor; therefore, imaging capability is an important consideration. Recently, designs of gamma detectors for prompt gamma-ray imaging have been proposed for online monitoring [5,7,8], but these are mostly based on simulation studies. In particular, there are no experimental studies that have successfully imaged 4.4-MeV gamma rays.

Our research group is developing a Compton camera based on a cerium-doped gadolinium aluminum gallium garnet (GAGG:Ce) scintillator, coupled with a multi-pixel photon counter (MPPC) [12,13]. In this experiment, however, we used a multi-anode photomultiplier (MAPMT) because the tolerance of the MPPC device at the beam facility under such radiation remains under investigation [14,15]. Herein, we present, for the first time, the preliminary results of an imaging test for 4.4-MeV prompt gamma rays, using a newly developed Compton camera.

A Compton camera utilizes the kinematics of Compton scattering to determine the direction of incident gamma rays, as given by

$$cos\theta_e = 1 - \frac{m_e c^2}{E_2} + \frac{m_e c^2}{E_1 + E_2}, \quad (1)$$

where E_1 denotes the energy of the recoil electron and E_2 denotes the energy of the scattered photon.

Fig. 5 shows the configuration of the Compton camera used for this experiment. The camera comprised a set of 3D-position-sensitive GAGG:Ce scintillator arrays [16] coupled to two MAPMT (HAMAMATSU, H12700A) that had 8 × 8 multi-anodes, each with dimensions of 6 mm×6 mm. The signals from the MAPMT were recorded with a head amp (CLEAR-PULSE, 80190) and data acquisition interface (CLEAR-PULSE, 80318). The data were acquired using LabVIEW. The pixels of the scintillator were separated by a 0.1-mm-thick reflective BaSO4 layer. The scatterer was an array of 20 pixels × 20 pixels × 5 pixels, and the absorber an array of 20 pixels × 20 pixels × 10 pixels. The resolution was 18.7° at 1332.5 keV at half maximum (full width at half maximum:FWHM).

Please cite this article in press as: A. Koide, et al., Spatially resolved measurement of wideband prompt gamma-ray emission toward on-line monitor for the future proton therapy, Nuclear Inst. and Methods in Physics Research, A (2017), https://doi.org/10.1016/j.nima.2017.10.020.

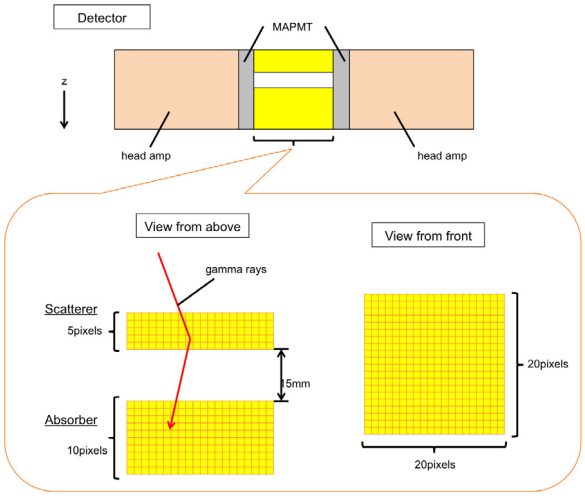

Fig. 5. Detector configuration of the Compton camera developed in this study.

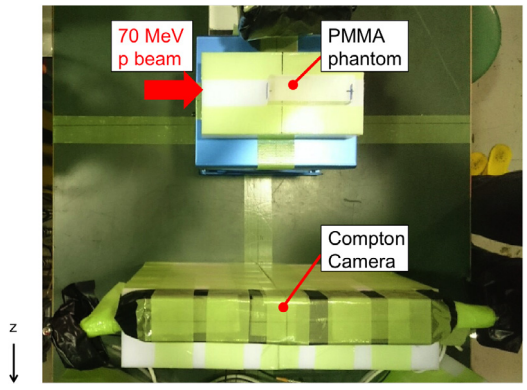

Fig. 6. Experimental geometry for an imaging test using a Compton camera.

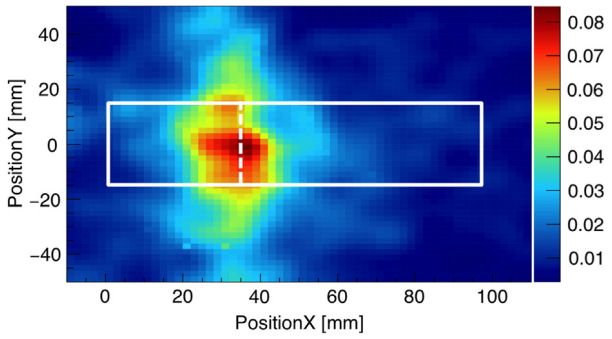

Fig. 7. 2D image of the 4.4-MeV prompt gamma rays reconstructed by the Compton camera. The white box indicates the PMMA phantom, and the dotted line marks the Bragg peak.

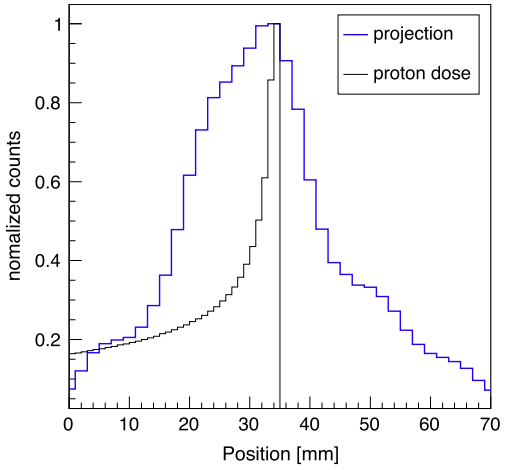

Fig. 8. A slice through the 2D image along the dotted line, as indicated in Fig. 7, comparing the 4.4-MeV gamma rays (*blue* line) with the proton dose distribution calculated by the Geant4 simulation code (*black* line). (For interpretation of the references to color in this figure legend, the reader is referred to the web version of this article.)

4.1. Experimental setup

We irradiated the PMMA phantom with a 70-MeV proton beam of intensity 0.3 pA. The distance between the Compton camera and the phantom was 18 cm as shown in Fig. 6. The center of the Compton camera's field of view was set at a 2-cm shift relative to the incidence of the proton beam, collimated to approximately 10 mm ϕ. The irradiation time was approximately 4 h. A long exposure time was required in this experiment because the low beam intensity was more than three orders of magnitude lower than a clinical therapy beam. In an actual clinical situation, imaging should be much faster with a higher-performance data acquisition system.

4.2. Result

Fig. 7 shows a preliminary image of 4.4-MeV prompt gamma rays reconstructed from 4366 events by the list-mode maximum likelihood expectation maximization (LM-MLEM) algorithm [13]. Fig. 8 shows a slice through the 2D image along the beam axis, over a range extending by 10 mm on either side of the Bragg peak. We set a wide energy window of 3–5 MeV, which includes the double and single escape peaks for the 4.4-MeV prompt gamma rays. The scatter energy window was set to 80 keV $\leq E_1 \leq$ 220 keV in order to reduce the incidence of backscattering events. Consequently, the peak was located at 33.3 ± 1.4 mm from the end surface of the PMMA phantom, thus coinciding with the Bragg peak. The image is blurred slightly owing to the limited angular resolution of the Compton camera, which is approximately 10° at the phantom position as measured at 4.4 MeV.

5. Discussion and conclusion

In this paper, we have systematically studied the spectra and spatial distributions of prompt gamma rays, using both simulations and experiments to mimic clinical proton beam irradiation. We conclude that, out of several potential energy windows, the window featuring the 4.4-MeV emission lines follows the dose distribution of protons most closely, consistent with the simulation predictions [7]. Moreover, we suggest that spatial distributions differ significantly depending on the choice of prompt gamma-ray emission line. A possible explanation is that each gamma-ray line has a different energy threshold for the relevant nuclear reaction channels. Indeed, prior research has indicated that the emission threshold for the 4.4-MeV prompt gamma rays is lower than that for other emission lines. In particular, for the case of proton beam irradiation, the emission threshold of the 4.4-MeV prompt gamma rays is 5 MeV, while that for the 718-keV prompt gamma rays is 30 MeV [10]. This explains why the 4.4-MeV gamma rays can be produced closer to the Bragg peak than other prompt gamma-ray emissions.

We confirm that the 1D distribution of 4.4-MeV gamma rays closely resembles the proton dose distribution, although contamination by scattered gamma rays would account for the difference between the simulation (Fig. 3) and the experimental profile (Fig. 4). Our preliminary experimental image, obtained using a Compton camera, corroborates this result. In a clinical setting, however, the proton energy most commonly used is 200 MeV, which has a longer range of 20–30 cm as a

Please cite this article in press as: A. Koide, et al., Spatially resolved measurement of wideband prompt gamma-ray emission toward on-line monitor for the future proton therapy, Nuclear Inst. and Methods in Physics Research, A (2017), https://doi.org/10.1016/j.nima.2017.10.020.

water-equivalent length, and our result should be verified with the 200-MeV beam. Moreover, we are developing a new method to effectively reduce multiple interactions in a detector which significantly degrades image quality.

Acknowledgment

This work was supported by JSPS KAKENHI Grant Number JP15H05720.

References

[1] T. Nishio, et al., Int. J. Radiat. Oncol. 76 (2010) 277–286.
[2] A.C. Kraan, et al., Nucl. Instrum. Methods A 786 (2015) 120–126.
[3] K. Parodi, et al., IEEE Trans. Nucl. Sci. 52 (2005) 778–786.
[4] M. Mashayekhi, et al., Rep. Pract. Oncol. Radiother. 22 (2017) 52–57.
[5] S. Kurosawa, et al., Curr. Appl. Phys. 12 (2012) 364–368.
[6] M. McCleskeya, et al., Nucl. Instrum. Methods A 785 (2015) 163–169.
[7] E. Hilaire, et al., Phys. Med. Biol. 61 (2016) 3127–3147.
[8] J. Smeets, et al., Phys. Med. Biol. 57 (2012) 3371–3405.
[9] P. Lopes, et al., Phys. Med. Biol. 60 (2015) 6063–6085.
[10] B. Kozlovsky, et al., Astrophys. J. Suppl. Ser. 141 (2002) 523–541.
[11] T. Sato, et al., J. Nucl. Sci. Technol. 50 (2013) 913–923.
[12] J. Kataoka, et al., Nucl. Instrum. Methods A 784 (2015) 248–254.
[13] T. Taya, et al., Nucl. Instrum. Methods A 831 (2016) 351–361.
[14] Z. Li, et al., Nucl. Instrum. Methods A 822 (2016) 63–71.
[15] V. Kushpil, et al., Phys. Conf. Ser. 675 (2016) 012039.
[16] A. Kishimoto, et al., IEEE Trans. Nucl. Sci. 60 (2011) 38–43.

Please cite this article in press as: A. Koide, et al., Spatially resolved measurement of wideband prompt gamma-ray emission toward on-line monitor for the future proton therapy, Nuclear Inst. and Methods in Physics Research, A (2017), https://doi.org/10.1016/j.nima.2017.10.020.